


2D and 3D Microstructural Reconstruction of Nodular Cast Iron

Caio Costa Abrantes Ferreira^a, André Luiz Moraes Alves^{b*} ,

Wesley Luiz da Silva Assis^a , Paulo Rangel Rios^a 

^aUniversidade Federal Fluminense, Escola de Engenharia Industrial Metalúrgica de Volta Redonda, Volta Redonda, RJ, Brasil.

^bUniversidade Federal do Rio de Janeiro, Programa/Departamento de Engenharia Metalúrgica e de Materiais, Rio de Janeiro, RJ, Brasil.

Received: September 15, 2023; Revised: March 05, 2024; Accepted: March 28, 2024

Reconstruction of random heterogeneous media has been an increasingly popular theme in materials science, as such media is primarily found in nature and manufactured materials. An ideal reconstruction includes every microstructural feature of the reference image and allows simulations of physical quantities that agree with experimental data. In this work, three 2D reconstructions and three 3D reconstructions are produced. All six are based on a single planar section. Its stereological and metallographic features are compared to those of the reference. 2D and 3D reconstructions from single planar sections were carried out with simulated annealing and a sampling method. The first reconstruction used the co-occurrence correlation function (CCF) and orthogonal sampling. The second employed the two-point correlation function (S_2) and the lattice point algorithm (LPA) as the sampling method. Finally, the third reconstruction used the S_2 together with the two-point cluster function (C_2) and the LPA as the sampling method. One of two sampling techniques (orthogonal and LPA) were used. The reconstructions that were done using S_2 and C_2 and LPA sampling provided the best results both in 2D and 3D cases, combining realistic morphology and good compatibility with the reference stereological measures.

Keywords: *Optimization, Simulated annealing, Heterogeneous media reconstruction, Microstructure, Characterization.*

1. Introduction

It is well-known that microstructure is a crucial issue in materials science. That is so because, to a considerable extent, macroscopic material properties, such as elasticity, yield strength, tensile strength, thermal and electrical conductivity, and fracture toughness, depend on the microstructure¹⁻⁴. Therefore, microstructural characterization and modeling are of particular interest.

Traditionally, one observes the microstructure on a planar section, whereas one typically seeks to determine three-dimensional microstructural quantities. A branch of mathematics, stereology, gives sound relationships between measures carried out on a planar section and certain three-dimensional features, such as volume fraction and interfacial area per unit of volume⁵. When full 3D reconstruction is required, a helpful technique is serial sectioning⁶⁻¹⁰, which measures consecutive planar sections with an approximately constant spacing. Earlier works used “manual” calculation^{6,7}, but later works greatly benefitted from computational reconstruction methods using the planar sections as input. Nonetheless, it would be highly desirable if one could reconstruct the 3D microstructure from measurements on a *single* planar section. We investigate this possibility and its limitations in the present paper.

The microstructure can be identified as a “random set,” “random heterogeneous material,” or “random media”^{11,12}. By random media, one means a geometric interpretation in a scale far greater than the molecular scale but much smaller than the size of the specimen. The generation of realizations, either 2D or 3D, of “random media” is a problem of considerable current interest in materials science and engineering and various areas of knowledge.

Specifically, in metallurgy and materials science, macroscopic properties such as elastic modulus, elasticity, yield, tensile strength, fracture toughness, and electrical and thermal conductivity are microstructure-dependent. For example, specific properties such as the elastic modulus are less sensitive to the defects in a single crystal. Still, the apparent elastic modulus may depend on the microstructure when two microstructural components with distinct elastic moduli are present¹⁻⁴. Therefore, the reconstruction of a random media must be sufficiently accurate to be the starting point of computer simulations to obtain the properties listed above.

Early reconstruction papers^{13,14} used autocorrelation, probability density, and Gauss filters to obtain a binary matrix. Oolitic calcarium and Fontainebleau arenite, chosen for their simple microstructure, are the first reconstructed random media. These methods presume isotropy and can only use the most straightforward correlation functions.

*e-mail: andrealves@metalmat.ufjf.br

Their extension to multiphase systems and anisotropic systems is complicated.

Rintoul and Torquato¹⁵ provided a better reconstruction methodology based on simulated annealing (SA). Those authors reported promising results for systems with low aggregation of pixels. However, Rintoul and Torquato concluded that even when there is good agreement between the reference correlation function and the correlation function obtained from the reconstructed microstructure, this does not necessarily imply that the reconstruction is faithful to the reference. Consequently, it is paramount to understand which correlation function is more satisfactory for each class of random media one wishes to reconstruct.

Torquato and Yeong¹⁶ extended previous work to heterogeneous random media in a seminal paper. According to Torquato and Yeong, the main advantages of their new formulation are: (a) easy implementation, (b) the possibility of using diverse correlation functions, and (c) adaptability to multiphase and anisotropic systems. Their algorithm is briefly described in the Methodology section below. Yeong-Torquato's method's main characteristic is its flexibility. Torquato's work and Chen et al.¹⁷ represent a class of reconstruction methods that employ optimization.

Other methods include multipoint statistics¹⁸⁻²⁰ that aim at decreasing computational costs. More recently, neural networks²¹⁻²⁴ have been employed. However, neural network models may take a long time to train. Nonetheless, they have the advantage that these models can quickly generate new microstructure realizations after training.

Several researchers have attempted to improve Yeong-Torquato's method²⁵⁻²⁷. Feng et al.'s²⁷ co-occurrence correlation function (CCF) described in the Background section below is one such attempt.

A critical point in microstructure reconstruction is determining the correlation function, for example, the two-point correlation function (S_2). A natural way of doing this is using the square or cubic lattice. For this reason, sampling in two orthogonal directions was initially employed. Torquato et al.²⁸ suggested a new way of sampling random media. They proposed a "lattice point algorithm" (LPA). This formalism can be used to determine the two-point correlation function but can be extended for the two-point cluster correlation function (C_2)²⁹.

In the present work, we employ the Yeong and Torquato¹⁶ and the Feng et al.²⁷ methods to reconstruct 2D and 3D microstructures of nodular cast iron. Feng et al.²⁷ method was chosen because it requires low computational resources compared to other methods. The reconstructions were carried out from a single reference 2D planar section of the nodular cast iron. Nodular cast iron is widely used in many applications, and its microstructure is relatively simple.

2. Background

2.1. Two-point correlation function

Let $I^{(j)}(\mathbf{r})$ be the indicator function of the j phase and \mathbf{r} the position of a matrix pixel, \mathbf{r}_1 and \mathbf{r}_2 are the endpoints of \mathbf{r} :

$$I^{(j)}(\mathbf{r}_1, \mathbf{r}_2) = 1, \text{ if } \mathbf{r}_1 \text{ and } \mathbf{r}_2 \text{ are within } j \text{ phase, or } 0 \text{ otherwise. (1)}$$

The two-point correlation function is defined by the probability, p_{ij} , of finding, \mathbf{r}_1 and \mathbf{r}_2 in phases i and j . Specifically, the two-point correlation function for phase j , $S_2^{(j)}(\mathbf{r}_1, \mathbf{r}_2)$, is the probability of finding \mathbf{r}_1 and \mathbf{r}_2 within the same phase j :

$$S_2^{(j)}(\mathbf{r}_1, \mathbf{r}_2) = \left\langle I^{(j)}(\mathbf{r}_1) I^{(j)}(\mathbf{r}_2) \right\rangle \quad (2)$$

where the angular brackets are symbols for mean value.

There are four possible two-point correlation functions, namely, $S_1^{(i)}(\mathbf{r}_1, \mathbf{r}_2)$, $S_2^{(j)}(\mathbf{r}_1, \mathbf{r}_2)$, and $S_{12}^{(ij)}(\mathbf{r}_1, \mathbf{r}_2) \equiv S_{21}^{(ji)}(\mathbf{r}_1, \mathbf{r}_2)$. Only one of these four is independent.

If the microstructure is statistically homogenous, the correlation function depends only on the *relative* positions of \mathbf{r}_1 and \mathbf{r}_2 . Moreover, if the microstructure is statistically isotropic, then the correlation function depends only on the distance between \mathbf{r}_1 and \mathbf{r}_2 :

$$S_2^{(j)}(\mathbf{r}_1, \mathbf{r}_2) = S_2^{(j)}(r) \quad (3)$$

where $r = |\mathbf{r}_1 - \mathbf{r}_2|$.

The relevant property of S_2 is that it is an even function. Therefore, for a square with $N \times N$ pixels (assuming periodic boundary conditions), one needs to calculate the function up to $r = N/2$ pixels. Figure 1a illustrates which endpoints belong to the two-point correlation function.

2.2. Two-point cluster correlation function

Let $I_C^{(j)}(\mathbf{r})$ be the indicator function of the j phase and \mathbf{r} the position of a matrix pixel, \mathbf{r}_1 and \mathbf{r}_2 are the endpoints of \mathbf{r} :

$$I_C^{(j)}(\mathbf{r}_1, \mathbf{r}_2) = 1, \text{ if } \mathbf{r}_1 \text{ and } \mathbf{r}_2 \text{ are within } j \text{ phase AND } \mathbf{r}_1 \text{ and } \mathbf{r}_2 \text{ are within the same cluster, or } 0 \text{ otherwise. (4)}$$

The two-point cluster correlation function of j phase can be defined as:

$$C_2^{(j)}(\mathbf{r}_1, \mathbf{r}_2) = \left\langle I_C^{(j)}(\mathbf{r}_1) I_C^{(j)}(\mathbf{r}_2) \right\rangle \quad (5)$$

For homogenous and isotropic microstructures:

$$C_2^{(j)}(\mathbf{r}_1, \mathbf{r}_2) = C_2^{(j)}(r) \quad (6)$$

Figure 1b illustrates which endpoints belong to the two-point cluster correlation function.

2.3. Lineal path function

Let $I_L^{(j)}(\mathbf{r}_1, \mathbf{r}_2)$ be the indicator function of the j phase and \mathbf{r} the position of a matrix pixel, \mathbf{r}_1 and \mathbf{r}_2 are the endpoints of \mathbf{r} :

$$I_L^{(j)}(\mathbf{r}_1, \mathbf{r}_2) = 1, \text{ if } \mathbf{r}_1 - \mathbf{r}_2 \text{ is fully contained within the same phase and cluster, or } 0 \text{ otherwise. (7)}$$

The two-point lineal path correlation function of j phase can be defined as:

$$I_2^{(j)}(\mathbf{r}_1, \mathbf{r}_2) = \left\langle I_L^{(j)}(\mathbf{r}_1) I_L^{(j)}(\mathbf{r}_2) \right\rangle \quad (8)$$

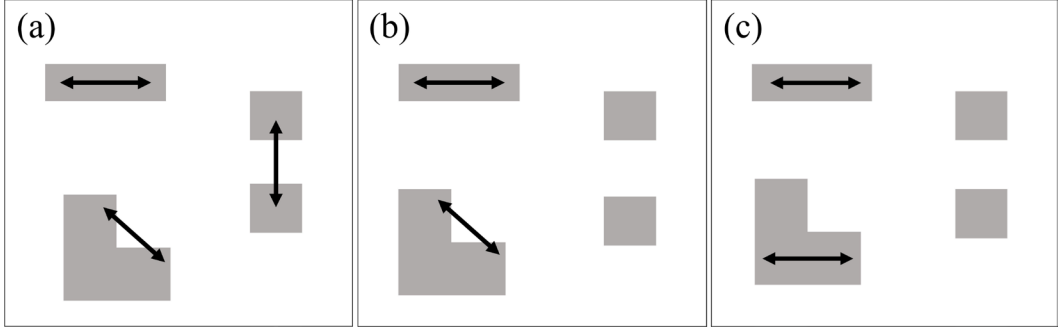


Figure 1. Examples of correlation functions. (a) Two-point correlation function of one phase. (b) Two-point cluster correlation function of one phase. (c) Two-point lineal path correlation function of one phase.

For homogenous and isotropic microstructures:

$$L_2^{(j)}(\mathbf{r}_1, \mathbf{r}_2) = L_2^{(j)}(r) \quad (9)$$

Figure 1c illustrates which endpoints belong to the two-point lineal path correlation function.

2.4. Co-occurrence correlation function

Feng et al.'s²⁷ co-occurrence correlation function can be defined as the probability, p_{ij} , of finding \mathbf{r}_1 and \mathbf{r}_2 in phases i and j :

$$\text{CCF}(x_1, x_2) = \begin{bmatrix} p_{11}(r) & p_{12}(r) \\ p_{21}(r) & p_{22}(r) \end{bmatrix} \quad (10)$$

For a homogeneous and isotropic microstructure $r = |\mathbf{x}_1 - \mathbf{x}_2|$ and one has a CCF(r).

Thus CCF(r) utilizes the four two-point correlation functions even though only one is independent. Results from Feng et al.²⁷ suggest that, among other advantages, CCF(r) represents connectivity information better than using a single function.

3. Methodology

The reconstructions are based on experimental results from Freitas³⁰ on nodular cast iron. One of Freitas's micrographs from a planar section is our reference micrograph. The micrograph was binarized. A matrix of 300×300 square grid represented the micrograph for the 2D reconstruction. A matrix of 122×122 square grid represented the binarized image for 3D reconstruction.

For the reconstruction, one considers that the nodular cast iron is a two-phase isotropic microstructure. A function, $f_0(r)$, is determined for the reference matrix, for example, the two-point correlation function. A matrix with random black and white cells is the starting point. Black represents the second phase, and white represents the "parent-matrix" phase. The volume fraction of the second phase in the reference micrograph is equal to the volume fraction of the second phase, black cells, in the matrix. The same function is applied to the starting matrix that evolves from its starting point to the reference matrix. At a certain time-step, k , this

evolution of the function f_S^k is calculated. A quantity E that may be considered the energy is determined by:

$$E_k = \sum_r \left[f_0 - f_S^k \right]^2 \quad (11)$$

For our matrix to evolve towards the reference matrix, thus minimizing E , one interchanges two randomly selected cells of distinct phases. Of course, this interchange does not change the volume fraction. After the interchange is conducted, the energy E_{k+1} is determined. The difference in energy between these two steps is $\Delta E = E_{k+1} - E_k$.

The Metropolis algorithm is used to accept the interchange or not:

$$p(\Delta E) = 1, \text{ if } \Delta E \leq 0 \quad (12)$$

$$p(\Delta E) = \exp\left(-\frac{\Delta E}{T}\right), \text{ if } \Delta E > 0 \quad (13)$$

where T is a "Monte Carlo temperature."

The objective of the reconstruction is that f_S^k reaches a value such that the energy is as close as possible to zero. Specific details of this method applied to the present case can be found in Ferreira³¹.

The simulated annealing was carried out here for the three functions defined in the Background section: the two-point correlation function (S_2); a combination of the S_2 and the two-point cluster correlation function (C_2); and the co-occurrence correlation function (CCF).

Two different sampling methods were used. The orthogonal sampling method and periodic boundary conditions were employed for the CCF²⁷. For the S_2 and for the combination of $S_2 + C_2$ the lattice point algorithm (LPA)²⁸ was used. When LPA was employed, one did not use periodic boundary conditions. We cropped the reconstructed matrix border by 5% to minimize border effects. Full details of the methodology can be found in Ferreira³¹.

4. Generation of 2D Microstructures from the Experimental Determination on a Single Plane

Figure 2 shows the microstructures generated by the 2D reconstructions from an experimental micrograph of nodular

cast iron. In what follows, qualitative observations resulting from a visual inspection are presented.

Using the CCF method, the reconstructed microstructure reproduces well the smaller nodules of the reference microstructure, shown in Figure 2a. The spatial distribution of the nodules also looks good. By contrast, the nodule's morphology in Figure 2b differs from those in Figure 2a. Figure 2b depicts elongated instead of equiaxed nodules. This behavior suggests that CCF performs well regarding the spatial distribution of nodules. Nonetheless, CCF falls short as far as connectivity/morphology information is concerned.

Figure 2c presents the reconstruction done by the S_2 method using the LPA sampling. It is apparent in Figure 2c that LPA sampling results in a rounded morphology of the nodules much better than the CCF method. Nevertheless, one can see some elongated nodules analogous to those of CCF, Figure 2b.

This result suggests that, like the CCF method, the S_2 method cannot preserve connectivity/morphology information well.

Figure 2d presents the microstructure reconstructed using a combination of S_2 and C_2 . Joint use of S_2 and C_2 results in a microstructure that closely approaches the reference microstructure, Figure 2a. The nodules have sizes and shapes similar to the experimental result. Few elongated nodules are present. All in all, the $S_2 - C_2$ method conveys a result better than the CCF and S_2 methods. The area per unit of volume, S_V , or equivalently, the mean intercept length are virtually the same, see Table 1.

Table 1 presents a quantitative summary of the above results. The volume fraction, V_V , is about the same for all three methods. It should be the same as it is kept constant in all three methods. The small difference is due to the 5% crop carried out in S_2 and $S_2 - C_2$ methods.

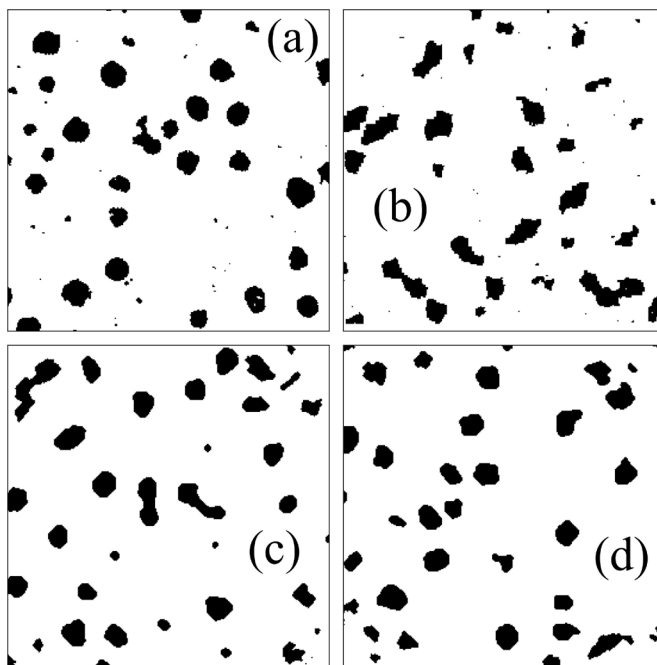


Figure 2. 2D reconstruction from a single experimental section, microstructures cut to final size 270×270 pixels. (a) Experimental-reference. (b) reconstruction using CCF. (c) reconstruction using S_2 . (d) hybrid reconstruction using $S_2 - C_2$.

Table 1. 2D reconstruction from a single experimental section: comparison of stereological measurements.

Measure	Reference	Reconstructions		
		CCF	S_2	$S_2 - C_2$
V_V	0.098	0.10	0.11	0.10
$N_A (\mu\text{m}^{-2})$	0.0011	0.0019	0.0012	0.0012
$S_V (\mu\text{m}^2 / \mu\text{m}^3)$	0.048	0.050	0.050	0.048
$\lambda (\mu\text{m})$	8.2	7.9	8.5	8.3
$F (\mu\text{m})$	10.4	6.8	10.8	10.1

The number of nodules per unit of area, N_A , and Feret diameter, F , using the S_2 and $S_2 - C_2$ methods are close to those of the experimental microstructure. In contrast, N_A and F obtained in the microstructure generated by the CCF method differ from the experimental microstructure. This confirms the result in Figure 2, which suggests that the CCF method gives the worst reconstruction. It is fair to say that the CCF method has the advantage of being much less computer-intensive than the S_2 and $S_2 - C_2$ methods besides it employs a worse sampling method, orthogonal sampling.

5. 3D Reconstruction of the Microstructure from a Single Experimental Section

Figure 3 shows the microstructures generated by 3D reconstructions from an experimental micrograph of nodular cast iron. Qualitative observations resulting from the visual inspection are presented in what follows. Figures 3b-3d are 2D sections of the 3D reconstructions. Those 2D sections are like those obtained by optical microscopy. They are compared with the reference microstructure in Figure 3a.

A comparison of the CCF reconstruction, Figure 3b, with the reference, Figure 3a, demonstrates that the CCF method cannot yield a nodule morphology resembling the experimental equiaxed nodule morphology. CCF nodules are not rounded, as is a typical graphite nodule. By contrast, the spatial distribution of the nodules looks reasonable. The reconstruction with the S_2 method results in a better morphology. An even better morphology can be obtained using the $S_2 - C_2$ method. Likewise, Figure 2 and Figure 3 suggest that the $S_2 - C_2$ method is the best of the three methods employed here. As mentioned above, the method utilizing

C_2 considerably improves the connectivity representation. The inclusion of C_2 causes a better reconstruction of the nodule's shape. Only an occasional elongated nodule is present compared to the CCF and S_2 methods.

Table 2 displays a quantitative summary comparing the three reconstruction methods. All three reconstruction methods gave comparable values. In other words, the planar section of the 3D reconstructions resulted in similar stereological quantities. In contrast to the reconstruction of the 2D sections shown above, Table 2 shows that the stereological measurements on the 2D sections of 3D reconstructions did not reflect the discrepancy observed in Figure 3 among the reconstruction methods.

Figure 4 displays a 3D opaque view of the reconstructions. Figures 4a-c exhibit a similar trend. Thus, the visually best reconstruction is obtained by $S_2 - C_2$ method. The following best is the method using S_2 followed by the CCF method, which presented the worst result of the three methods.

The trend observed in Figure 4 becomes clearer using 3D views of the reconstructions. Figures 5a-c show transparent views of the reconstructions. The transparent views reinforce that the reconstruction is worse with CCF improves with S_2 and becomes much better with the $S_2 - C_2$ method. The reconstruction is inferior to the CCF method. The shape of the nodules is far from the approximately spherical shape of the graphite nodules. The shape improves somewhat, but it still is not satisfactory with the S_2 method. Finally, the $S_2 - C_2$ method results in a significant improvement.

6. Discussion

The CCF method is closely related to the two-point correlation functions of the microstructure²⁷. According to

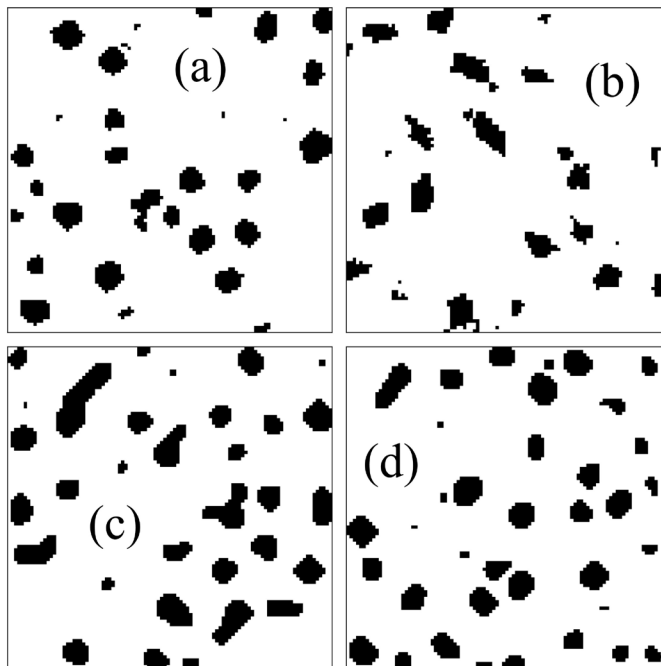
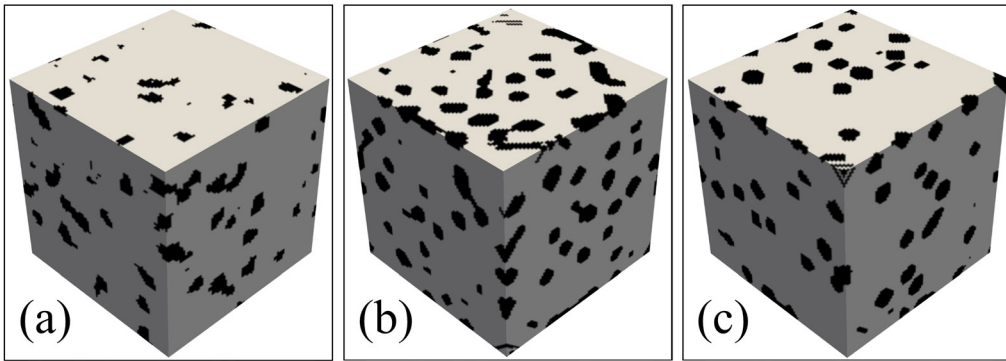
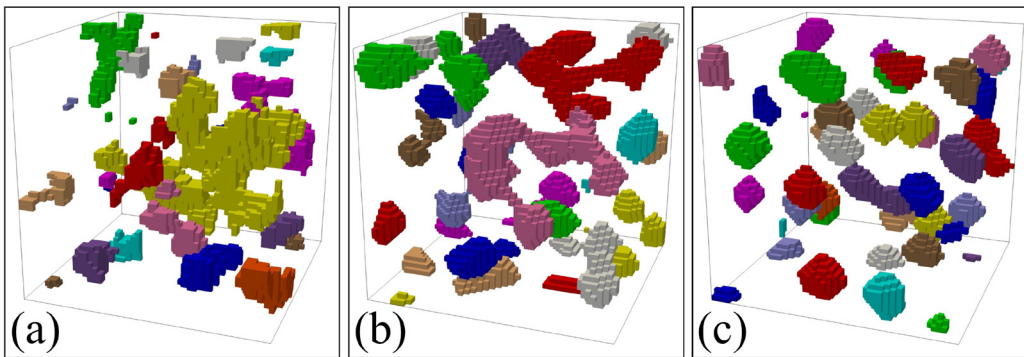


Figure 3. 2D sections of 3D reconstructions from a single experimental section. (a) Experimental-reference. (b) reconstruction using CCF. (c) reconstruction using S_2 . (d) hybrid reconstruction using $S_2 - C_2$.

Table 2. 3D reconstruction from a single experimental section: comparison of stereological measurements.

Measure	Reference	Reconstructions		
		CCF	S_2	$S_2 - C_2$
V_V	0.10	0.10	0.10	0.10
$N_A (\mu\text{m}^{-2})$	0.0012	0.0012	0.0011	0.0012
$S_V (\mu\text{m}^2 / \mu\text{m}^3)$	0.042	0.044	0.043	0.044
$\lambda (\mu\text{m})$	9.3	9.3	9.3	9.1
$F (\mu\text{m})$	10.0	10.5	10.5	10.0

**Figure 4.** 3D opaque views of the reconstructions. (a) reconstruction using CCF. (b) reconstruction using S_2 . (c) hybrid reconstruction using $S_2 - C_2$.**Figure 5.** 3D transparent views of the reconstructions. (a) reconstruction using CCF. (b) reconstruction using S_2 . (c) hybrid reconstruction using $S_2 - C_2$.

Feng et al.²⁷, the CCF method gives better reconstruction results than a method that uses the S_2 function only, as done here. Nonetheless, the results obtained here appear to indicate otherwise. The results from the CCF used here do not contradict Feng et al.'s²⁷ statement. This is because the sampling method used for CCF and S_2 methods were different. As described in the Methodology section, for CCF, one used orthogonal sampling, whereas for S_2 the LPA was used. This algorithm compensated a likely worse reconstruction when one uses the S_2 function only.

Still, a better sampling algorithm was not enough to cause a satisfactory result using solely the S_2 function. Further microstructural information is required. For this reason, we added the C_2 function to the S_2 function to get the $S_2 - C_2$ method. The inclusion of the C_2 function improved connectivity information, and the overall results were better than those obtained by the CCF and the S_2 methods.

Figure 6 supports this reasoning for the 2D reconstructions. Figure 6 depicts the lineal path correlation function of the

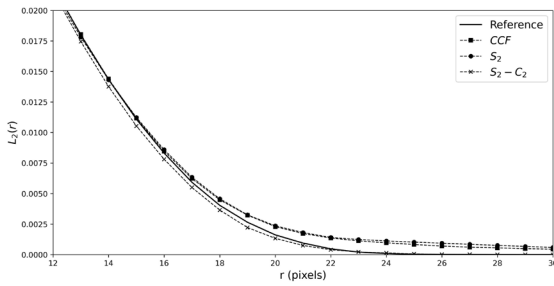


Figure 6. Comparison of $L_2(r)$ values for 2D reconstructions from a single experimental section.

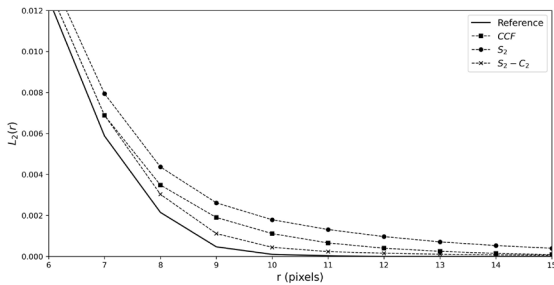


Figure 7. Comparison of $L_2(r)$ values for 3D reconstructions from a single experimental section.

reconstructions by the three methods. This graph distinctly shows that the $S_2 - C_2$ method gives the best results.

For the 3D reconstructions, Figure 7 corroborates $S_2 - C_2$ method better representation of connectivity. In Figure 7, likewise in Figure 6, the connectivity, the L_2 function approaches that of the reference as the method changes from CCF, S_2 to the $S_2 - C_2$ method.

Nevertheless, Figure 7 demonstrates that the $S_2 - C_2$ method does possess a $L_2(r)$ that is closer to the reference $L_2(r)$ than the other methods but remains some distance from the reference $L_2(r)$.

Therefore, our results suggest that even if the $S_2 - C_2$ method produced a reasonable reconstruction, the combination of S_2 and C_2 is unable to thoroughly represent all microstructural information from the nodular cast iron reference micrograph.

7. Conclusions

The Yeong-Torquato¹⁶ method applied to a nodular cast iron's 2D and 3D microstructural reconstruction showed promising results. The quality of results varies according to the correlation functions and sampling method used in each case.

Stereological measurements typical of 2D reconstructions using S_2 and $S_2 - C_2$ were compatible with the experimental-reference microstructure.

The 3D reconstructions using CCF, S_2 and $S_2 - C_2$ presented interesting results. The best reconstruction was obtained by $S_2 - C_2$ method, followed by the S_2 method, and the CCF method, which presented the worst result of the three methods. The same trend was obtained in the 2D reconstructions. However, our results

suggest that although the methods produced a reasonable reconstruction, they could still not reproduce the complete microstructural information from the nodular cast iron reference micrograph. Despite that, even with some degree of uncertainty, they may be helpful to the researcher to get information and inferences from just one experimental planar section, with a relatively easy implementation and low computational cost.

Our results also demonstrate that the reconstruction technique proposed by Yeong and Torquato¹⁶ shows a wide possibility of use in metallurgical and materials engineering. Using this method associated with other techniques may bring even better results in the future as new correlation functions and sampling techniques can be developed.

8. Acknowledgments

This study was financed in part by the Coordenação de Aperfeiçoamento de Pessoal de Nível Superior - Brasil (CAPES) - Finance Code 001. The authors are also grateful to Conselho Nacional de Desenvolvimento Científico e Tecnológico, CNPQ, and Fundação Carlos Chagas Filho de Amparo à Pesquisa do Estado do Rio de Janeiro, FAPERJ, for the financial support. The authors gratefully acknowledge the Center for Computational Materials Science, Institute for Materials Research, Tohoku University for the use of MASAMUNE-IMR (Materials science Supercomputing system for Advanced Multi-scale simulations towards Next-generation - Institute for Materials Research) supercomputer. In particular, the authors are grateful to Professors Yayoi Terada and Tetsuo Mohri for their collaboration through the Global Institute for Materials Research Tohoku (GIMRT) program.

9. References

1. Oberwinkler B. Modeling the fatigue crack growth behavior of Ti-6Al-4V by considering grain size and stress ratio. *Mater Sci Eng A*. 2011;528(18):5983-92. <http://doi.org/10.1016/j.msea.2011.04.046>.
2. Ghosh A, Sivaprasad S, Bhattacharjee A, Kar SK. Microstructure-fracture toughness correlation in an aircraft structural component alloy Ti-5Al-5V-5Mo-3Cr. *Mater Sci Eng A*. 2013;568:61-7. <http://doi.org/10.1016/j.msea.2013.01.017>.
3. Xu J, Zeng W, Zhao Y, Jia Z. Effect of microstructure evolution of the lamellar alpha on impact toughness in a two-phase titanium alloy. *Mater Sci Eng A*. 2016;676:434-40. <http://doi.org/10.1016/j.msea.2016.09.017>.
4. Shao H, Zhao Y, Ge P, Zeng W. Crack initiation and mechanical properties of TC21 titanium alloy with equiaxed microstructure. *Mater Sci Eng A*. 2013;586:215-22. <http://doi.org/10.1016/j.msea.2013.08.012>.
5. Russ JC, Dehoff RT. *Practical stereology*. 2nd ed. New York: Kluwer Academic/Plenum Publishers; 2000.
6. Núñez C, Domingo S. Statistical considerations on uniform grain size. *Metall Trans, A, Phys Metall Mater Sci*. 1988;19(12):2937-44. <http://doi.org/10.1007/BF02647720>.
7. Krauss G, Marder AR. The morphology of martensite in iron alloys. *Metall Trans*. 1971;2(9):2343-57. <http://doi.org/10.1007/BF02814873>.
8. Velichko A, Mücklich F. Quantitative 3D characterisation of graphite morphology in cast iron: correlation between processing, microstructure and properties. *Int J Mater Res*. 2009;100(8):1031-7. <http://doi.org/10.3139/146.110148>.

9. Kral MV, Mangan MA, Spanos G, Rosenberg RO. Three-dimensional analysis of microstructures. *Mater Charact.* 2000;45(1):17-23. [http://doi.org/10.1016/S1044-5803\(00\)00046-2](http://doi.org/10.1016/S1044-5803(00)00046-2).
10. Baldissera MR, Rios PR, Hein LRO, Sandim HRZ. Three-dimensional characterization of pores in Ti-6Al-4V alloy. *Mater Res.* 2011;14(1):102-6. <http://doi.org/10.1590/S1516-14392011005000014>.
11. Rios PR, Villa E. Transformation kinetics for inhomogeneous nucleation. *Acta Mater.* 2009;57(4):1199-208. <http://doi.org/10.1016/j.actamat.2008.11.003>.
12. Jiao Y, Stillinger FH, Torquato S. Modeling heterogeneous materials via two-point correlation functions: I. Basic principles. *Phys Rev E Stat Nonlin Soft Matter Phys.* 2007;76:031110. <http://doi.org/10.1103/PhysRevE.76.031110>.
13. Quiblier JA. New three-dimensional modeling technique for studying porous media. *J Colloid Interface Sci.* 1984;98(1):84-102. [http://doi.org/10.1016/0021-9797\(84\)90481-8](http://doi.org/10.1016/0021-9797(84)90481-8).
14. Adler PM, Jacquin CG, Quiblier JA. Flow in simulated porous media. *Int J Multiph Flow.* 1990;16(4):691-712. [http://doi.org/10.1016/0301-9322\(90\)90025-E](http://doi.org/10.1016/0301-9322(90)90025-E).
15. Rintoul MD, Torquato S. Reconstruction of the structure of dispersions. *J Colloid Interface Sci.* 1997;186(2):467-76. <http://doi.org/10.1006/jcis.1996.4675>.
16. Yeong CLY, Torquato S. Reconstructing random media. *Phys Rev E Stat Phys Plasmas Fluids Relat Interdiscip Topics.* 1998;57(1):495-506. <http://doi.org/10.1103/PhysRevE.57.495>.
17. Chen D, Teng Q, He X, Xu Z, Li Z. Stable-phase method for hierarchical annealing in the reconstruction of porous media images. *Phys Rev E Stat Nonlin Soft Matter Phys.* 2014;89(1):013305. <http://doi.org/10.1103/PhysRevE.89.013305>.
18. Tahmasebi P, Sahimi M. Reconstruction of three-dimensional porous media using a single thin section. *Phys Rev E - Stat Nonlinear. Soft Matter Phys.* 2012;85:066709.
19. Hajizadeh A, Safekordi A, Farhadpour FA. A multiple-point statistics algorithm for 3D pore space reconstruction from 2D images. *Adv Water Resour.* 2011;34(10):1256-67. <http://doi.org/10.1016/j.advwatres.2011.06.003>.
20. Okabe H, Blunt MJ. Prediction of permeability for porous media reconstructed using multiple-point statistics. *Phys Rev E Stat Nonlin Soft Matter Phys.* 2004;70:066135.
21. Feng J, Teng Q, Li B, He X, Chen H, Li Y. An end-to-end three-dimensional reconstruction framework of porous media from a single two-dimensional image based on deep learning. *Comput Methods Appl Mech Eng.* 2020;368:113043. <http://doi.org/10.1016/j.cma.2020.113043>.
22. Mosser L, Dubrulle O, Blunt MJ. Reconstruction of three-dimensional porous media using generative adversarial neural networks. *Phys Rev E.* 2017;96(4):043309. <http://doi.org/10.1103/PhysRevE.96.043309>.
23. Bostanabad R, Bui AT, Xie W, Apley DW, Chen W. Stochastic microstructure characterization and reconstruction via supervised learning. *Acta Mater.* 2016;103:89-102. <http://doi.org/10.1016/j.actamat.2015.09.044>.
24. Zhang F, He X, Teng Q, Wu X, Dong X. 3D-PMRNN: reconstructing three-dimensional porous media from the two-dimensional image with recurrent neural network. *J Petrol Sci Eng.* 2022;208:109652. <http://doi.org/10.1016/j.petrol.2021.109652>.
25. Tang T, Teng Q, He X, Luo D. A pixel selection rule based on the number of different-phase neighbours for the simulated annealing reconstruction of sandstone microstructure. *J Microsc.* 2009;234(3):262-8. <http://doi.org/10.1111/j.1365-2818.2009.03173.x>.
26. Ju Y, Huang Y, Zheng J, Qian X, Xie H, Zhao X. Multi-thread parallel algorithm for reconstructing 3D large-scale porous structures. *Comput Geosci.* 2017;101:10-20. <http://doi.org/10.1016/j.cageo.2017.01.003>.
27. Feng J, Teng Q, He X, Qing L, Li Y. Reconstruction of three-dimensional heterogeneous media from a single two-dimensional section via co-occurrence correlation function. *Comput Mater Sci.* 2018;144:181-92. <http://doi.org/10.1016/j.commatsci.2017.11.030>.
28. Jiao Y, Stillinger FH, Torquato S. A superior descriptor of random textures and its predictive capacity. *Proc Natl Acad Sci USA.* 2009;106(42):17634-9. <http://doi.org/10.1073/pnas.0905919106>.
29. Torquato S, Beasley JD, Chiew YC. Two-point cluster function for continuum percolation. *J Chem Phys.* 1988;88(10):6540-7. <http://doi.org/10.1063/1.454440>.
30. Freitas AFP. Metalografia quantitativa tridimensional dos ferros fundidos nodular e cinzento [dissertation]. Volta Redonda: Universidade Federal Fluminense; 2008.
31. Ferreira CCA. Reconstrução microestrutural 2D e 3D de ferro fundido nodular pelo método de Yeong-Torquato [dissertation]. Volta Redonda: Universidade Federal Fluminense; 2021.